Eurographics Symposium on Rendering 2003
Per Christensen and Daniel Cohen-Or (Editors)

# Efficient Isotropic BRDF Measurement

Wojciech Matusik,[1] Hanspeter Pfister,[2] Matthew Brand,[2] and Leonard McMillan[3]

[1] Laboratory for Computer Science, MIT, Cambridge, Massachusetts, USA
[2] Mitsubishi Electric Research Labs, Cambridge, Massachusetts, USA
[3] University of North Carolina at Chapel Hill, Chapel Hill, North Carolina, USA

**Abstract**

*In this paper we present novel reflectance measurement procedures that require fewer total measurements than standard uniform sampling approaches. First, we acquire densely sampled reflectance data for a large collection of different materials. Using these densely sampled measurements we analyze the general surface reflectance function to determine the local signal variation at each point in the function's domain. We then use wavelet analysis to derive a common basis for all of the acquired reflectance functions as well as a corresponding non-uniform sampling pattern that corresponds to all non-zero wavelet coefficients. Second, we show that the reflectance of an arbitrary material can be represented as a linear combination of the surface reflectance functions. Furthermore, our analysis provides a reduced set of sampling points that permits us to robustly estimate the coefficients of this linear combination. These procedures dramatically shorten the acquisition time for isotropic reflectance measurements. We present a detailed description and analysis of our measurement approaches and sampling strategies.*

## 1. Introduction

Modeling and measuring how light is reflected from surfaces is a central theme in both computer graphics and computer vision. The Bidirectional Reflectance Distribution Function (BRDF) describes reflection under the assumption that all light transport occurs at a single surface point. Measured BRDF data allows the generation of photorealistic images and is important for many image analysis tasks. Furthermore, measured BRDF data can also be used to refine BRDF models, and these improved models can aid the measurement process.

A general BRDF describes reflected radiance as a four-dimensional function of incident and exitant directions. In this paper we focus on the important subclass of *isotropic* BRDFs, for which rotations about the surface normal can be ignored. Isotropic BRDFs can be described by a three-dimensional function of the incident angle from the surface normal and the reflected radiance over the entire hemisphere. A uniform sampling of this function requires a huge amount of measurements. For example, an angular resolution of $0.5^\circ$ requires more than 46 million measurements.

The classical device for measuring BRDFs is the gonioreflectometer, which is composed of a photometer and light source that are moved relative to a surface sample under computer control. By design, such devices measure a single radiance value at a time, making this process very time-consuming. There have been efforts to make this acquisition process more efficient by measuring many BRDF samples at once. This can be achieved by using a digital camera and mirrors[22, 3] or spherical samples of the measured material[14]. However, optical elements usually do not allow the measurement of reflectance at near grazing angles, and they can be a source of indirect illumination, which can corrupt the measurements. BRDF measurements using spherical specimens may be difficult for some materials, and this approach requires the material to be homogeneous. In either case, a dense sampling of the BRDF still requires numerous high-dynamic range photographs and a lot of time.

Our work tries to reduce the number of BRDF measurements by answering these questions: (1) What is the required sampling frequency over the domain of the isotropic BRDF function to adequately measure it? (2) What is the optimal set of basis functions that represent any isotropic BRDF? (3) Can new BRDFs be represented as a linear combinations of these basis functions? The answer to these questions leads to optimal BRDF sampling procedures for gonioreflectometers and digital camera scanners.

Our techniques are based on the measurement and anal-

ysis of a relatively large collection of densely sampled isotropic BRDFs from many different materials[15]. Our first proposed measurement procedure is based on the wavelet analysis of the space of measured BRDFs. We observe that the BRDF functions in our set have varying frequency content at various points in their domain. For example, specular highlights have complicated local spectrums that contain high frequencies, whereas off-specular signals are typically smooth with simple local spectrums. We exploit these properties of BRDF spectrums to derive an efficient measurement procedure that employs a non-uniform sampling of the BRDF function. The sampling density at each point of the function's domain is proportional to the signal frequency that adequately represents any BRDF. This technique requires around 69,000 measurements at specific points of the BRDF domain.

Next, we show that new BRDFs can be accurately represented using a linear combination of 100 BRDFs in the originals set. It follows that one needs only 100 measurements to derive coefficients for the linear combination. This modeling procedure requires having the original densely sampled BRDFs to synthesize the new BRDFs. We show that the noise and error characteristics of the BRDFs synthesized using this method are very good.

## 2. Background and Previous Work

Compared to the vast literature on BRDF models, there are relatively few publications about BRDF measurements. Traditionally, BRDF data is measured using gonioreflectometers[17, 1]. One of the first methods to use a digital camera is the pioneering work of Ward[22]. His measurement device consists of a hemispherical mirror and a camera with a fisheye lens. Moving the light source and material over all incident angles enables the measurement of anisotropic BRDF data.

Dana et al.[4] developed a system to measure spatially varying BRDFs, also called Bidirectional Texture Functions (BTFs). Using a digital camera, a robot arm, and a light source, they take approximately 200 reflectance measurements over varying incident and reflected angles for a planar material sample. The data for about 60 measured materials is available as the CUReT database[2]. More recently, they proposed an improved measuring device for BTFs using a parabolic mirror[3].

Marschner et al.[14, 13] constructed an efficient measurement system for isotropic BRDFs by using a spherical material sample. A fixed camera takes images of the sample under varying illumination from an orbiting light source. We use a similar setup, discussed in Section 3, to measure a large database of isotropic BRDFs. Lu et al.[12] use a similar scanning device with cylindrical sample geometry to measure the anisotropic BRDF of velvet. Marschner et al. extended their method to surface geometry acquired with a laser range scanner, including human faces[14]. None of these measuring approaches take the local spectral characteristics of BRDFs into account. Consequently, they all require a dense, uniform sampling over the BRDF domain, which is time and data intensive.

To shorten the acquisition procedure, and to filter out the inherent noise of the measurement process, measured BRDF data is typically fit to analytic BRDF models using various optimization techniques[22, 8, 4, 14]. Sato et al.[19] fit a spatially varying BRDF model to the relatively sparse image data of a rotating object with known geometry from laser range measurements. Lensch et al.[11] improve this approach by clustering sparsely sampled reflectance measurements, fitting a Lafortune BRDF model[8] to the data, and then computing basis BRDF functions for material clusters using principal function analysis (PFA). Yu et al.[24] fit an analytic BRDF model to scenes that include global effects, such as indirect illumination. However, analytic BRDF functions are only an approximation of real reflectance, and the resulting analytic model is only an approximate fit to the measured BRDF values.

There are a variety of BRDF representations that have been used for fitting measured data. Westin et al.[23] proposed spherical harmonics to fit simulated BRDF data. Lafortune et al.[8] developed a compact BRDF model based on cosine lobes that is able to represent off-specular peaks and retro-reflection. Schroeder at al.[20] use spherical wavelets to represent a slice of the BRDF with constant viewing direction. Other efficient representations include Zernicke polynomials[7], purely positive matrix factorization[16], and singular value decomposition (SVD)[6].

Lalonde and Fournier[9, 10] use a wavelet decomposition and a wavelet coefficient tree to represent BRDFs. The major advantage of wavelets is the ability to perform local analysis – that is, to analyze a localized area of a larger signal. As we will show in Section 4, we employ a similar wavelet tree representation for our large collection of measured isotropic BRDFs.

## 3. Data Acquisition

We have built a BRDF measurement device similar to the one described by Marschner et al.[13] (see Figure 1). Our device and its measurement process are described in detail by Matusik et al.[15].

Our acquisition system, like Marschner's, requires a spherical specimen of each material that is measured. We have acquired isotropic BRDFs of more than 100 different materials, including metals, plastics, painted surfaces, and fabrics. Figure 2 depicts some of the materials that were acquired. We used this corpus of sampled BRDFs to analyze the general signal characteristics of isotropic BRDFs. This analysis, in turn, allowed us to derive optimal sampling

**Figure 1:** A photograph of our isotropic BRDF measurement device.

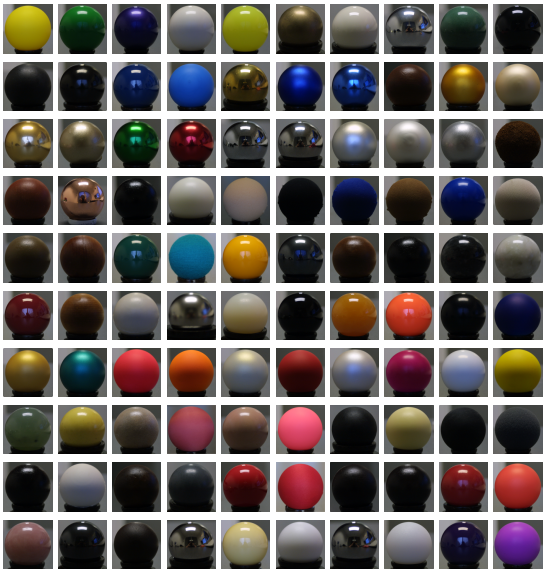

**Figure 2:** Pictures of some acquired materials.

strategies for subsequent BRDF measurements, under the assumption that our measured BRDFs are representative of the space of all isotropic BRDFs.

## 4. BRDF Representation

The natural coordinate system ($\theta_{in}$, $\theta_{out}$, $\phi_{diff}$) for isotropic BRDFs requires very dense angular sampling to accurately represent specular peaks. When the sampling frequency for any angle is too low, a circular specular peak may become an ellipse tilted in different directions depending on the incoming light position.

To address this problem we use the coordinate system proposed by Rusinkiewicz[18] (Figure 3) which parameterizes BRDFs based on the half-vector between incoming and outgoing light direction. The three angles used to describe

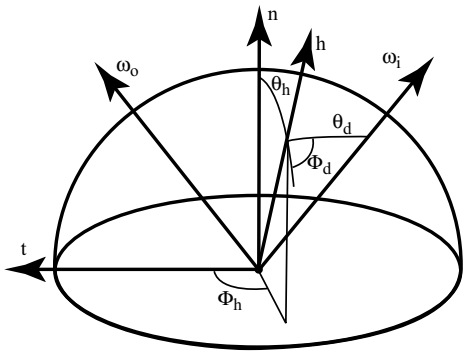


**Figure 3:** The Rusinkiewicz BRDF coordinate system.

isotropic BRDF are: $\theta_h$, $\theta_d$, and $\phi_d$. The angle $\phi_h$ is irrelevant for isotropic BRDFs.

We make use of nonuniform sampling to represent the specular peaks more efficiently. Specifically, we sample $\theta_h$ more densely near the specular reflection and decrease the sampling density as the angle increases. We illustrate this in Figure 4) for one incident light direction.

In our BRDF measurement method, each image of a sphere specimen represents many BRDF samples[15]. We put all measurements corresponding to the same angles $(\theta_h, \theta_d, \phi_d)$ into so called sampling bins. To minimize systematic noise, we remove the lowest and highest 25% of the values in each sampling bin and average the remaining measurements. This also helps to compensate for small variations in material properties over the specimen.

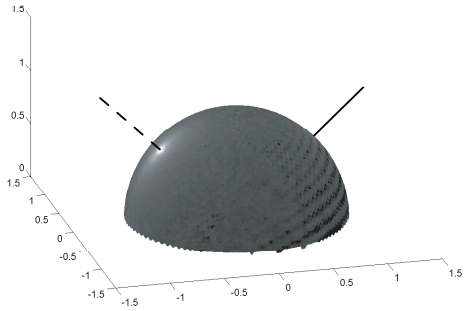

**Figure 4:** Our sampling density for one slice of a BRDF ($\theta_{in}$ = 45°). The solid line denotes the incident light direction. The sampling density is the highest (white color) near the specular reflection direction (dashed line).

We discretize $\theta_h$, $\theta_d$, and $\phi_d$ into 90, 90, and 360 sampling bins, respectively. This results in a total of 90 x 90 x 360 = 2,916,000 bins for each color component (R,G,B). We also enforce the BRDF reciprocity constraint, which in the Rusinkiewicz coordinate system takes the form of:

$$f(\theta_h, \theta_d, \phi_d) = f(\theta_h, \theta_d, \phi_d + \pi). \quad (1)$$

By taking advantage of reciprocity we need only discretize $\phi_d$ into 180 bins. Overall, the Rusinkiewicz BRDF parameterization reduces the number of sampling bins required to represent specular BRDFs with a given fidelity. We estimate that we would need samples every $0.25^\circ$ in the natural coordinate system (23,328,000 sampling bins for each color channel) to comparably represent the same BRDFs.

Subsequent analysis of the localized frequency content of our acquired BRDF database will permit us to even further reduce the sampling density of our BRDFs. The details of this analysis and the resulting implications for BRDF sampling strategies are described in the following sections.

## 5. Wavelet Analysis of BRDFs

Typical BRDFs exhibit high frequencies in only very specific regions of their parameter space (e.g., near specular peaks). Only these regions require dense radiance sampling. Otherwise, BRDFs are smooth and slowly varying over most of their domain, and, thus, require fewer samples for accurate reconstruction in these regions. As discussed in the previous section, non-uniform sampling can be used to exploit this "spatially varying" localized spectrum property, which is characteristic of BRDFs. The precise densities and patterns of this non-uniform sampling is largely a matter of guess work, and it is likely that one should err on the side of oversampling the function, as we attempted to do in our acquisition of example BRDFs. However, once given a large set of oversampled representative BRDFs it is possible to analyze the entire corpus in order to reveal the maximum localized signal frequencies for any point in the domain, which in turn implies the maximum necessary sampling frequency for that point. Assuming that our example BRDFs are representative of the entire space of isotropic BRDFs, we can then sample the BRDF of any new material correctly at a lower non-uniform sampling rate without any a priori knowledge.

Standard Fourier analysis could be used to determine the frequency spectrum of our database. However, the maximum signal frequency would be very high since the Fourier basis functions span the whole domain of the sample space. Consequently, a Fourier analysis would suggest a dense and uniform sampling. We instead use wavelet analysis to obtain the maximum signal frequency for each part of the BRDF domain. The advantage of wavelet analysis is its ability to perform localized analysis of a larger signal because the underlying wavelet basis functions vary both in the spatial and in the frequency domain[21].

Wavelets have been used before to represent BRDFs. Schröder and Sweldens[20] use spherical wavelets to represent 2D slices of a 4D reflectance function. They can represent a slice of the BRDF with several hundreds of coefficients (the rest of the coefficients is set to zero). Lalonde and Fournier[10] extended this work and represent 4D reflectance functions using 4D basis wavelet functions stored in a wavelet tree. They achieve a very compact representation for a single BRDF. In our work we use a wavelet tree to analyze and represent our entire collection of measured BRDF functions.

Wavelet analysis represents a particular BRDF function as a linear combination of basis functions of varying scale. At the same time it specifies the signal frequency over each interval of the function's domain that is required to represent the function. The signal frequency translates directly to the required sampling frequency for each interval[21]. In general, this sampling frequency is only adequate for one particular BRDF. We performed a wavelet analysis for all of the BRDFs we have measured. For each interval of the BRDF domain we found the maximum required frequency needed in order to reconstruct any of the measured BRDFs. Using this information we derive the sampling density (and corresponding sampling points $(\theta_h, \theta_d, \phi_d)$) which should be measured in order to sample any arbitrary BRDF correctly. Our algorithm also reconstructs a dense BRDF representation from the measured BRDF values at the specified sampling points.

We now discuss the details of our wavelet analysis. As stated in Section 4, each measured BRDF is represented as a $90 \times 90 \times 180$ three-dimensional array of sampling bins. Standard wavelet analysis packages require data dimensions that are powers of two. We insert each BRDFs into a $256 \times 256 \times 256$ array and pad the rest of the array with zeros. Next, we perform a non-uniform wavelet transform on each 3D array to obtain an array of $256 \times 256 \times 256$ wavelet coefficients. For each BRDF, we keep the highest coefficients that allow us to reconstruct the BRDF with 3% precision because that is the estimated accuracy of our measurements[15]. The rest of the coefficients are set to zero.

The non-zero wavelet coefficients define the required signal frequency in each interval of the domain for a particular BRDF. The set of non-zero coefficients is generally different for each measured BRDF. However, there is a large degree of coherence between these sets. When we take the union of these sets for all 100 BRDFs, the size of the set grows to approximately 69,000 common wavelet coefficients – 4.7% of the original data. The union of non-zero coefficients corresponds to a set of wavelet functions. We call this set of wavelet functions the *Common Wavelet Basis (CWB)* for all isotropic BRDFs. This wavelet basis defines the maximum signal frequency over each interval of the function's domain for all BRDFs in our set.

Next, we discuss how to define the BRDF sampling points, how to compute the CWB coefficients using the BRDF values at these sampling points, and how to reconstruct the full BRDF from the CWB. First, we note that each BRDF $G(\theta_h, \theta_d, \phi_d)$ can be represented as a weighted sum of the CWB functions $H_i(\theta_h, \theta_d, \phi_d)$ as follows:

$$G(\theta_h, \theta_d, \phi_d) = \sum_{i=1}^{n} H_i(\theta_h, \theta_d, \phi_d) \times C_i, \qquad (2)$$

where $C$ is a vector of coefficients for the CWB functions that need to be computed. We also note that all of the CWB functions are known (for the sake of simplicity we use Haar wavelets) and they can be evaluated at any point $(\theta_h, \theta_d, \phi_d)$. Each BRDF value $G(\theta_h, \theta_d, \phi_d)$ produces one linear constraint on the values of the wavelet coefficients $C$. Given the approximately 69,000 non-zero coefficients as constraints allows us to compute all wavelet coefficients $C$ by solving a system of linear equations.

Next, we need to select the sampling points $(\theta_h, \theta_d, \phi_d)$ that produce the linearly independent equations, and, therefore, allow us to compute the wavelet coefficients. We note that there is no unique set of sampling points; thus, we just select one possible set that leads to linearly independent equations. First, we compute one constraint for each original sampling point for a total of 1,458,000 equations. Many of these are linearly dependent. We determine a set of 69,000 equations that are linearly independent. Given these equations and the corresponding BRDF values we solve the following system of equations:

$$G = H \times C. \tag{3}$$

Matrix $H$ is large (69,000 $\times$ 69,000) but typically very sparse – usually there are around 40 nonzero elements in a row. This is a result of the small support of the wavelets at higher levels in the wavelet tree. We use the MATLAB sparse matrix routine to directly perform the operation $H^T / C^T$ for each color channel (R, G, and B).

Unfortunately, the coefficients for wavelets at the lowest levels (level 0, 1, and 2) are not estimated robustly. There are 8, 84, and 384 of them, respectively. However, we can estimate these coefficients using a different method. We collapse the sparse 69,000 BRDF values from a 256 $\times$ 256 $\times$ 256 grid to a 16 $\times$ 16 $\times$ 16 grid by averaging the values. This grid becomes completely filled and we perform the wavelet transform on this low resolution grid. The coefficients of the low resolution grid approximate the low level coefficients of the high resolution grid well.

In order to reconstruct a BRDF we use the estimated coefficients of the CWB and we set coefficients for the wavelets not in the CWB to zero. Then we perform the inverse wavelet transform to compute the BRDF values at the original sampling grid locations.

## 6. Pull-Push Reconstruction of BRDFs

In the previous section we have shown how to reconstruct a BRDF on a uniform grid using 69,000 BRDF samples at specified locations. In this section, we present an alternative reconstruction method that in practice yields lower reconstruction errors.

Since we are given sparse BRDF samples we can treat the problem of reconstructing the full grid BRDF as a scattered data interpolation problem. One simple and fast methods is the pull-push method[5]. This method relies on the pyramid data structure of a progressively downsampled BRDF.

The algorithm consists of two steps. (1) The *pull* step is applied hierarchically from the highest to the lowest resolution in the BRDF pyramid. Each lower resolution of the pyramid is obtained from the higher resolution version. First, the higher resolution BRDF is convolved with a low pass filter. Then, the result of this convolution is downsampled by a factor of two to obtain the lower resolution BRDF. (2) The *push* step is also applied hierarchically to the BRDF pyramid. It starts at the lowest resolution and progresses to the highest, original, resolution. Low resolution data computed during the *pull* phase is used to fill in the gaps at the higher resolution. If the higher resolution BRDF value has high enough confidence then the lower resolution value is not used. Otherwise, the higher and lower resolution values are blended together. The implementation details of the algorithm are described by Gortler et al.[5].

## 7. Linear Combinations of BRDFs

Matusik et al.[15] performed Principal Component Analysis (PCA) over the set of more than 100 densely measured BRDFs. They have shown that each of the measured BRDFs can be represented well by a linear combination of 45 principal components. In this section we show that new BRDFs can be represented equally well using the BRDFs in the original set. It follows that one needs only to estimate appropriate weighting factors for each of the original BRDFs in order to estimate any new BRDF. Since there are only 100 of these coefficients, the number of BRDF samples needed for this estimation should be relatively small.

We represent each densely sampled BRDF as a high-dimensional vector composed of all values for R, G, and B. Let $P$ be the matrix of all BRDFs in the original set, $C$ the vector of coefficients for the linear combinations, and $B$ the new BRDF we measure. It follows that:

$$P \times C \approx B. \tag{4}$$

This system of equations is over-constrained since it has 90 $\times$ 90 $\times$ 180 $\times$ 3 = 4,374,000 equations and only 100 unknowns. However, a lot of these equations are linearly dependent. Therefore, we need to select only a small set of equations that allows us to robustly estimate the coefficients $C$.

Let $X$ be a matrix composed of some subset of rows of the matrix $P$. A good measure of how robustly we can estimate $C$ is the ratio between the highest and lowest eigenvalue of the matrix $X^T X$. The system is well conditioned if this ratio is small. Since finding an optimal set exhaustively is prohibitive, we resort to a simple greedy strategy. We start with an initial set of $n$ constraints. We select a constraint outside of the set $X$ and one constraint in the set $X$. We swap them only if the ratio of the eigenvalues decreases in matrix $X^T X$

with the constrains swapped. We repeat this procedure till $X$ converges to a stable set and we perform this procedure for different set sizes $n$.

This procedure guarantees that the system is numerically well conditioned, which in turn makes it robust to perturbations of the constraints. It also approximates a "most informative set" of measurements. In order to expect good generalization of the known BRDFs, we must also ensure that the system is well overconstrained. From large deviation theory, we can expect that the number of measurements necessary grows with the square root of the number of unknowns. Typically, a small multiple is sufficient for linear systems. We found out using $n = 800$ linear constraints ensures robust computation of the coefficients while adding more constraints does not improve the solution. This implies that we can measure any BRDF using only 800 samples. At each point we measure either R, G, or B. We note that each of the 800 equations corresponds to a specific value of $(\theta_h, \theta_d, \phi_d)$ and does not depend on the value of the BRDF at that point.

The procedure presented here is well defined, simple, and fast. In order to compute the coefficients $C$ we only need to compute a pseudo-inverse of the $800 \times 100$ matrix and perform one vector-matrix multiply. In contrast to fitting samples to analytical BRDF models this procedure is not dependent on a good initial guess.

## 8. Results

To validate our methods, we densely measured four additional isotropic BRDFs: dark-red paint, gold paint, orange plastic, and aluminum-bronze. These materials are substantially different from any of the materials in the original collection.

First, we show that these BRDFs can be represented well using only the coefficients in the CWB (which of course has been computed without these materials). Figure 5 compares the original BRDFs and the BRDFs expressed with the CWB for different angles of incident illumination. The errors for each of the BRDFs are: dark-red paint - 0.7%, gold paint - 0.9%, orange plastic - 2.1%, and aluminum-bronze - 1.2%. We conclude that our common wavelet basis represents these new BRDFs well.

Next, we reconstruct these BRDFs from 69,000 samples specified by the linear constraints. The results of this reconstructions are shown in Figure 6. The errors for each of the reconstructed BRDFs compared to the original BRDFs are: dark-red paint - 1.0%, gold paint - 1.3%, orange plastic - 3.2%, and aluminum-bronze - 1.2%. Although the errors are relatively small we observe some ringing artifacts that are typical for the non-smooth Haar wavelets. Smooth wavelets should yield better looking results.

We also reconstruct the same BRDFs using the pull-push algorithm. We use the same 69,000 sparse BRDF samples. This solution yields better results. The errors for each of the pull-push reconstructed BRDFs compared to the original BRDFs are: dark-red paint - 0.6%, gold paint - 0.9%, orange plastic - 2.5%, and aluminum-bronze - 1.1%. The results of the pull-push reconstructions are shown in Figure 7.

Next we show that the reflectance of these materials can be represented well using a linear combination of 100 BRDFs from the original collection (which also did not contain these BRDFs). In Figure 8 we show the comparison between the original densely sampled BRDFs and the corresponding reconstructed BRDFs using just 800 BRDF samples. The errors for each of the reconstructed BRDFs as a linear combination of BRDFs compared to the original BRDFs are: dark-red paint - 1.8%, gold paint - 1.8%, orange plastic - 4.3%, and aluminum-bronze - 2.5%.

All methods have their advantages and disadvantages. Both the CWB and the pull-push reconstruction require 69,000 measurements. However, these methods are independent of any BRDF database and can be applied immediately. The linear combination of BRDFs requires only 800 measurements, but it relies on the availability of the BRDF database.

## 9. Conclusions and Future Work

In this paper we have presented two novel approaches for measuring isotropic BRDFs. These procedures significantly reduce the number of required measurement samples. The reflectance functions reconstructed using our procedures approximate the exhaustively measured reflectances well.

One obvious extension of this work is to apply a similar approach to full 4D reflectance functions of anisotropic materials. The wavelet analysis of the arbitrary reflectance functions might also find use in efficient rendering algorithms.

We used the simplest wavelet function (Haar) to perform wavelet analysis which is not optimal for BRDF representations. We plan to investigate the use of other wavelet basis functions to perform our analysis.

## Acknowledgments

We would like to thank Markus Gross for insightful discussions and Paul Lalonde for making his wavelet shader available. Parts of this work were supported by NSF CAREER grant 9875859.

## References

1. Cornell light measurement laboratory. http://www.graphics.cornell.edu/research/measure/. 2
2. Curet: Columbia-utrech reflectance and texture database. http://www.cs.columbia.edu/CAVE/curet/. 2
3. K. Dana. BRDF/BTF measurement device. *ICCV*, pages 460–466, 2001. 1, 2

4. K. J. Dana, B. van Ginneken, S. K. Nayar, and J. J. Koenderink. Reflectance and texture of real world surfaces. *ACM Transactions on Graphics*, 1(18):1–34, 1999. 2

5. S. Gortler, R. Grzeszczuk, R. Szeliski, and M. Cohen. The lumigraph. *Computer Graphics*, 30(Annual Conference Series):43–54, 1996. 5

6. J. Kautz and M. McCool. Interactive rendering with arbitrary BRDFs using separable approximations. In *Rendering Techniques '99 (Proceedings of the Tenth Eurographics Workshop on Rendering)*, pages 281–292, New York, NY, June 1999. Springer Wien. 2

7. J. Koenderink, A. van Doorn, and M. Stavridi. Bidirectional Reflection Distribution Function expressed in terms of surface scattering modes. *European Conference on Computer Vision*, pages 28–39, 1996. 2

8. E. Lafortune, S.-C. Foo, K. Torrance, and D. Greenberg. Non-linear approximation of reflectance functions. *Computer Graphics*, 31(Annual Conference Series):117–126, 1997. 2

9. P. Lalonde and A. Fournier. Filtered local shading in the wavelet domain. In J. Dorsey and P. Slusallek, editors, *Rendering Techniques '97 (Proceedings of the Eighth Eurographics Workshop on Rendering)*, pages 163–174, New York, NY, 1997. Springer Wien. 2

10. P. Lalonde and A. Fournier. A wavelet representation of reflectance functions. *IEEE Transactions on Visualization and Computer Graphics*, 3(4):329–336, 1997. 2, 4

11. H. Lensch, J. Kautz, M. Goesele, W. Heidrich, and H.-P. Seidel. Image-based reconstruction of spatially varying materials. In *Proceedings of the 12th Eurographics Workshop on Rendering*, pages 104–115, June 2001. 2

12. R. Lu, J. Koenderink, and A. Kappers. Optical properties (Bidirectional Reflectance Distribution Functions) of velvet. *Applied Optics*, 37(25):5974–5984, September 1998. 2

13. S. Marschner, S. Westin, E. Lafortune, and K. Torrance. Image-based measurement of the Bidirectional Reflectance Distribution Function. *Applied Optics*, 39(16):2592–2600, June 2000. 2

14. S. Marschner, S. Westin, E. Lafortune, K. Torrance, and D. Greenberg. Image-based BRDF measurement including human skin. In *Proceedings of the 10th Eurographics Workshop on Rendering*, pages 139–152, Granada, Spain, June 1999. 1, 2

15. W. Matusik, H. Pfister, M. Brand, and L. McMillan. A data-driven reflectance model. *Computer Graphics*, 37(Annual Conference Series), 2003. 2, 3, 4, 5

16. M. McCool, J. Ang, and A. Ahmad. Homomorphic factorization of BRDFs for high-performance rendering. *Computer Graphics*, 35(Annual Conference Series):171–178, 2001. 2

17. Nist reference reflectometer: Starr facility. http://physics.nist.gov/. 2

18. S. Rusinkiewicz. A new change of variables for efficient BRDF representation. In G. Drettakis and N. Max, editors, *Rendering Techniques '98 (Proceedings of Eurographics Rendering Workshop '98)*, pages 11–22, New York, NY, 1998. Springer Wien. 3

19. Y. Sato, M. D. Wheeler, and K. Ikeuchi. Object shape and reflectance modeling from observation. volume 31, pages 379–387, 1997. 2

20. P. Schröder and W. Sweldens. Spherical wavelets: Efficiently representing functions on the sphere. *Computer Graphics*, 29(Annual Conference Series):161–172, 1995. 2, 4

21. G. Strang and T. Nguyen. *Wavelets and Filter Banks*. Wellesley-Cambridge Press, 1996. 4

22. G. Ward. Measuring and modeling anisotropic reflection. *Computer Graphics*, 26(Annual Conference Series):265–273, 1992. 1, 2

23. S. Westin, J. Arvo, and K. Torrance. Predicting reflectance functions from complex surfaces. *Computer Graphics*, 26(Annual Conference Series):255–264, 1992. 2

24. Y. Yu, P. Debevec, J. Malik, and T. Hawkins. Inverse global illumination: Recovering reflectance models of real scenes from photographs. *Computer Graphics*, 33(Annual Conference Series):215–224, 1999. 2

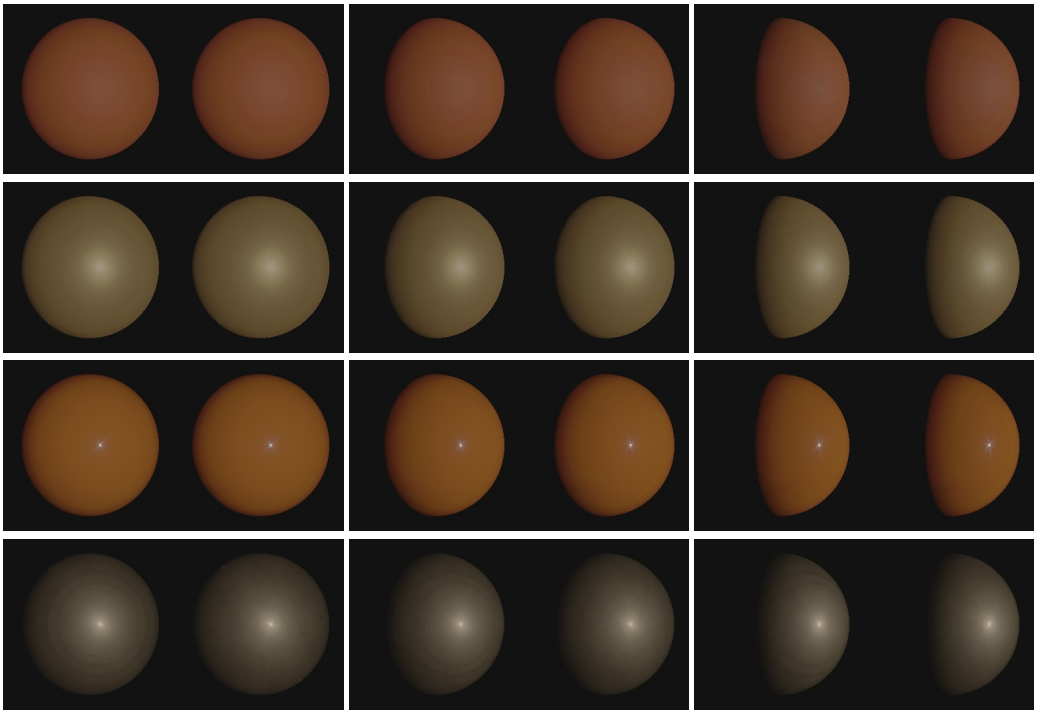

**Figure 5:** Comparison of BRDFs expressed in common wavelet basis (left) with original densely sampled BRDFs (right). Each row shows a different BRDF (first row - dark-red paint,second row - gold paint, third row - orange plastic, fourth row - aluminium-bronze).

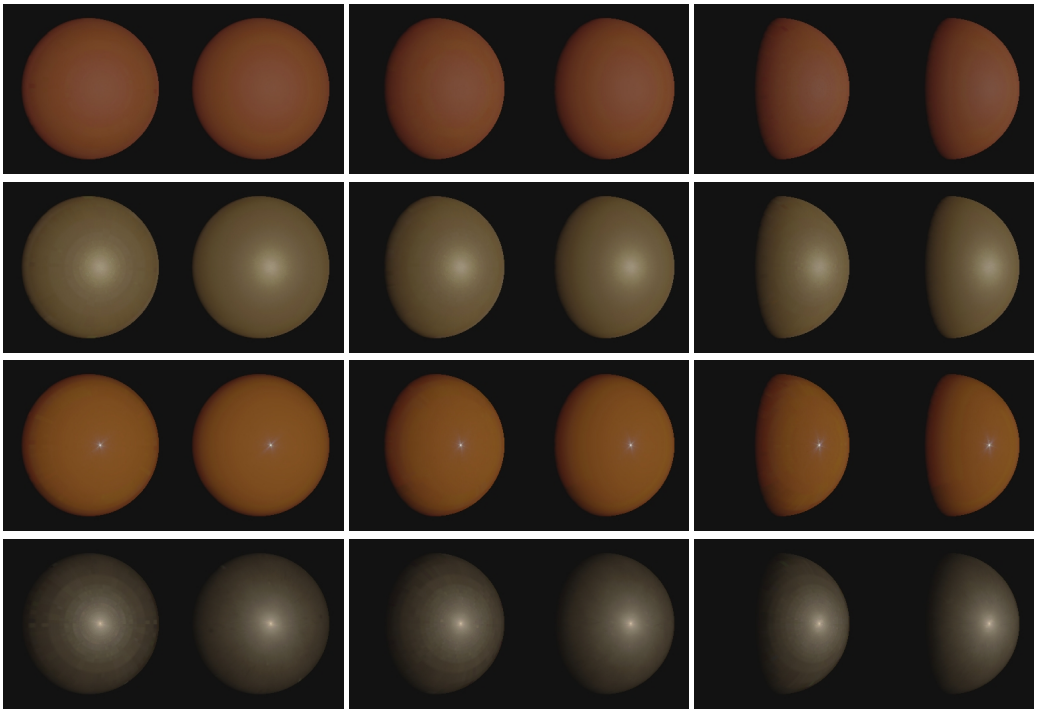

**Figure 6:** Comparison of wavelet reconstructed BRDFs using 69,000 sparse samples (left) with the original densely sampled BRDFs (right) (first row - dark-red paint,second row - gold paint, third row - orange plastic, fourth row - aluminum-bronze).

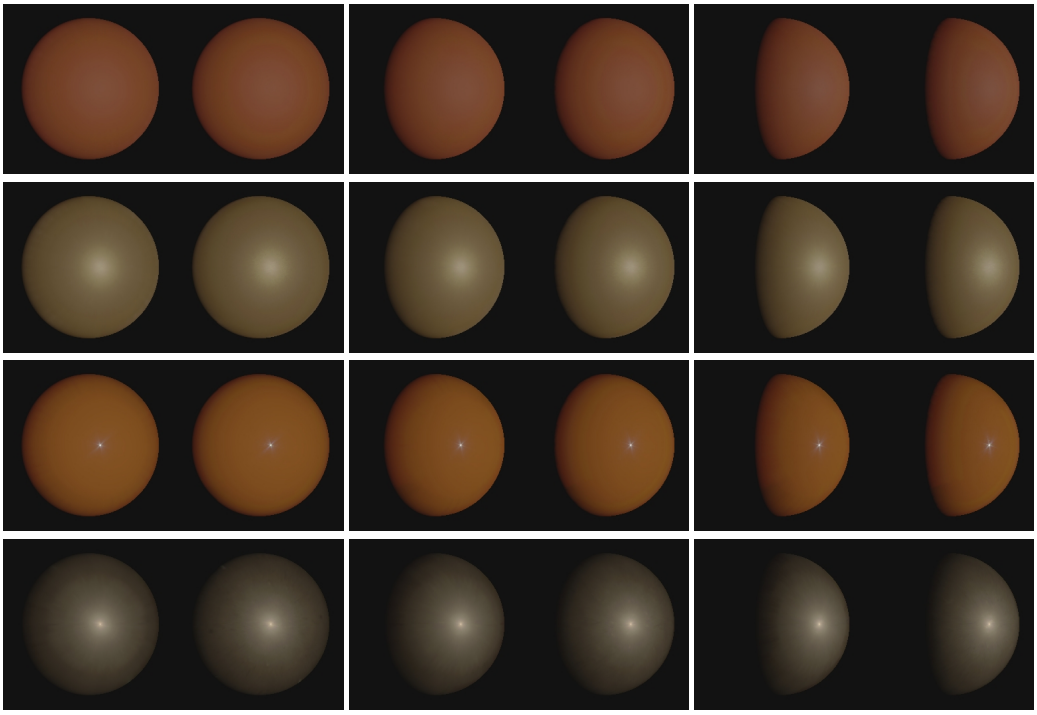

**Figure 7:** Comparison of pull-push reconstructed BRDFs using 69,000 sparse samples (left) with the original densely sampled BRDFs (right) (first row - dark-red paint,second row - gold paint, third row - orange plastic, fourth row - aluminum-bronze).

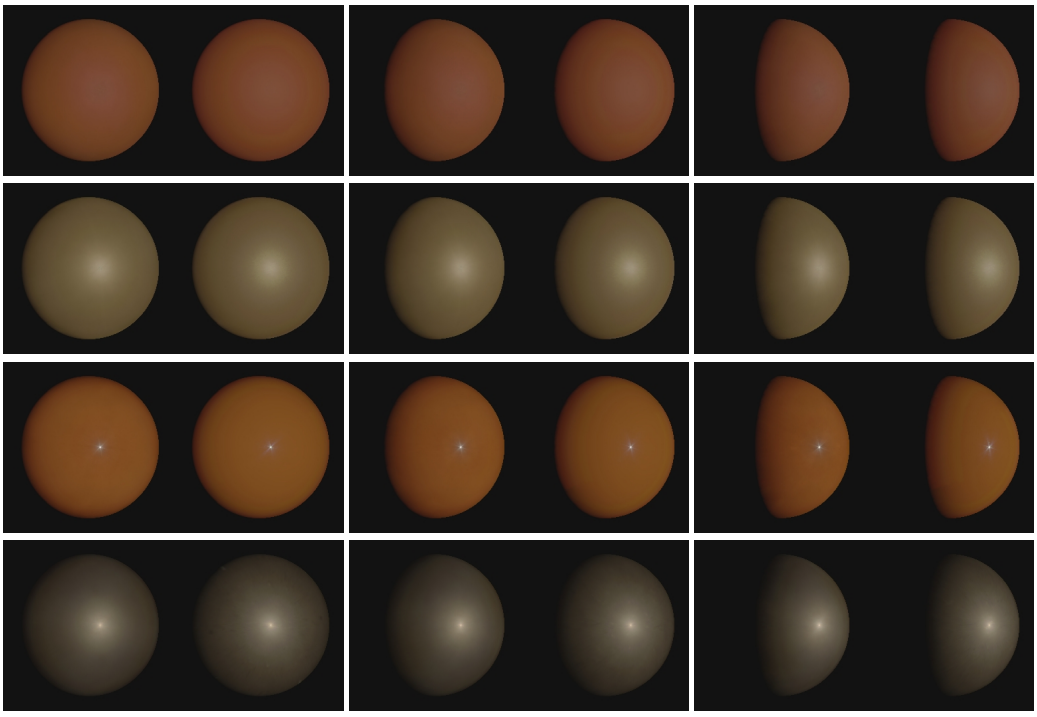

**Figure 8:** Comparison of BRDFs reconstructed as linear combinations of original BRDFs using 800 samples (left) with original densely sampled BRDFs (right). Each row shows a different BRDF (first row - dark-red paint, second row - gold paint, third row - orange plastic, fourth row - aluminum-bronze).